Core Precession and Global Modes in Granular Bulk Flow

Denis Fenistein, Jan-Willem van de Meent, and Martin van Hecke
Kamerlingh Onnes Lab, Leiden University, Post Office box 9504, 2300 RA Leiden, Netherlands
(Received 23 July 2005; published 21 March 2006)

We report a novel transition to core precession for granular flows in a split-bottomed shear cell. This transition is related to a qualitative change in the 3D flow structure: For shallow layers of granular material, the shear zones emanating from the split reach the free surface, while for deep layers the shear zones meet below the surface, causing precession. The surface velocities reflect this transition by a change of symmetry. As a function of layer depth, we find that three qualitatively different smooth and robust granular flows can be created in this simple shearing geometry.

DOI: 10.1103/PhysRevLett.96.118001 PACS numbers: 45.70.−n, 83.50.Ax, 83.85.Cg

Slowly sheared granular matter usually organizes into rigid regions separated by narrow shear bands where the material yields and flows [1–5]. Such grain flows appear to prohibit successful continuum modeling—not only because of the steep gradients in velocity, but also because subtle microscopic characteristics of the granulate can alter the flow in a qualitative manner [3].

We recently showed that the formation of narrow shear bands can be avoided by driving the granulate from a discontinuity in the bottom support of the grain layer [Fig. 1(a)], which effectively pins a wide shear zone away from the sidewalls [6–8]. The resulting grain flows are smooth and robust, with both velocity profiles and the location of the shear zones exhibiting simple, grain independent properties. These flows should be amenable to a continuum description, which forms an important motivation for their detailed study [6–8]. The two crucial parameters of this system are the location R_s of the slip in the bottom support, and the thickness of the granular layer H [Fig. 1(a)]. When H/R_s is small, the core material rests on the stationary center disc, and these flows have been characterized recently [6,7]. With increasing H, the width of these shear zones grows continuously, and their location moves inward toward the central region [6]. This implies that for *deep* layers new phenomena can be expected to occur.

Figures 1(b)–1(f) illustrate the novel flow patterns that are characteristic for *deep* layers. The most striking feature is that the core now *precesses* with a constant rate—hence material in the central part of the surface no longer rests on the disc. Precession is not simply the consequence of the overlap of two opposing shear zones, since before being eroded by shear, the inner core rotates as a solid blob for an appreciable time [Figs. 1(b)–1(f)]. A more intricate mechanism is at play here.

In this Letter we will characterize this transition to precession. We first address how the precession rate grows with layer depth, and relate precession to a qualitative change in the 3D structure of the flow field. We then show how this change is reflected in a change of the symmetry of the *surface* velocity profiles. The location of the shear zone at the surface for deep layers is compared to an empirical scaling law [6] and a recent theory [7]. Finally, we employ the rich structure of the shear zones for deep layers to establish that a crucial characteristic mesoscopic length scale, which sets the width of the shear zones, grows as a nontrivial power law with layer depth.

Setup.—Our setup is a modified version of the disk geometry described in earlier work [6], and consists of a stationary bottom disk of radius R_s, a rotating bottom ring, and an outer cylinder of radius 105 mm [Fig. 1(a)]. The disc radius R_s can be varied from 45 mm to 95 mm. The cell is filled to a height H with a polydisperse mixture of spherical glass beads with diameters ranging from 0.6 to 0.8 mm; a layer of grains is glued to the side walls and bottom rings to obtain rough boundaries. No segregation could be observed, and the free surface remains essentially flat. The surface velocities are recovered by a variant of

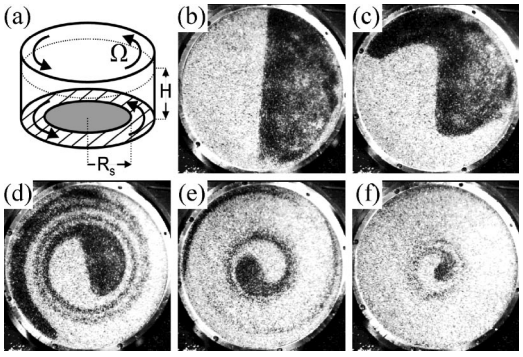

FIG. 1. Core precession in a split-bottomed geometry. (a) Schematic side-view of our split-bottomed shear cell, showing the layer height H (indicated by dotted line), a stationary bottom disk of radius R_s (gray), the bottom ring (striped), and outer cylinder of radius 105 mm that rotate with rate Ω. (b), (c), (d), (e), (f) Series of snapshots of top views of our setup (for $R_s = 95$ mm, $H = 60$ mm, and rotation rate $\Omega = 0.15$ rad/s), where colored particles sprinkled on the surface illustrate the core precession for $t = 0$ s (b), $t = 10$ s (c), $t = 10^2$ s (d), $t = 10^3$ s (e), and $t = 10^4$ s (f).

particle image velocimetry [6]. Transients are short and average velocities are azimuthal and proportional to the driving rate Ω. We represent the velocity profiles as $\omega(r)$, the ratio of the average angular surface velocity, and Ω, where r is the radial coordinate and Ω is fixed at 0.15 rad/s. Because ω is a ratio of a velocity and r, data taken for $r < 20$ mm is unreliable and omitted from the analysis.

Precession.—We define the precession rate ω_p as the limit of $\omega(r)$ for r going to zero. As explained above, ω cannot be measured reliably for small r. Nevertheless, $\omega(r)$ levels off for small radius, and in practice we fit a smooth function to $\omega(r)$ to estimate ω_p—various functions gave very comparable results (see below). For various slip radii, the onset height for precession grows with R_s [Fig. 2(a)], and the data for ω_p collapses when plotted as a function of H/R_s [Fig. 2(b)]. Note that when H/R_s becomes of order one, the whole surface rotates rigidly and $\omega_p \to 1$. Our data is consistent with recent results in a similar setup where the disc was rotated and the outer cylinder kept fixed [8].

3D flow structure.—The flow in the bulk has been probed by putting patterns of lines of colored tracer particles at given height in the bulk, adding more material, rotating the system for a short period (~8 s), and recovering the deformed pattern by carefully removing the upper layers of grains. In Fig. 3, two examples of the 3D flow patterns illustrate that for shallow layers the shear zones that emanate from the split in the bottom reach the free surface, thus leading to a stationary core, while for deep layers the shear zones (partially) meet in the bulk, leading to precession of the core.

In a recent theory by Unger *et al.*, the shear zones are modeled as infinitely thin sliding sheets. This model predicts that for shallow layers the shear sheet reaches the free surface but that for deep layers the shear sheet closes in the bulk of the material, and that a hysteretic transition between these two states occurs for $H/R_s \approx 0.65$ [7]. Figure 3 illustrates that this change in the shear zones with increasing height is also observed experimentally. However, the model cannot capture the smooth velocity fields observed experimentally and predicts a hysteretic jump between $\omega_p = 0$ and $\omega_p = 1$, while our data shows a smooth, nonhysteretic crossover.

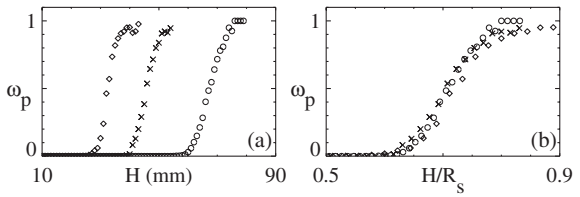

FIG. 2. (a) Precession rate ω_p as a function of H for $R_s = 45$ mm (diamonds), $R_s = 65$ mm (×) and $R_s = 95$ mm (circles). (b) Data collapse when ω_p is plotted as a function of H/R_s.

Recent MRI studies and numerical simulations evidence that in the crossover regime where $0 \ll \omega_p \ll 1$, the 3D flow structure can be conceived as having two shear zones—one reaching the free surface and one closing in the bulk [8]. The relative amount of shear across these two zones is set by the layer depth—for shallow layers the vertical shear zones dominate and ω_p is small, for deeper layers the horizontal shear zones increase in strength and ω_p increases accordingly. Extending the sliding sheet model [7] by taking disorder into account, Kertész *et al.* have reached a similar conclusion [9].

Surface velocities.—In the remainder of this Letter, we will focus on the *surface* velocities in the transitory regime, which can be measured much more accurately than bulk flow. Vertical gradients of the velocity are small near the surface, so that what is observed at the surface is not substantially different from what happens in the top layers [6–8]. For shallow layers, we established in Ref. [6] that $\omega(r)$ is well fitted by

$$\omega(r) = \mathrm{nerf}\left(\frac{r - R_c}{W}\right), \tag{1}$$

where R_c and W parameterize the location and width of the shear zones, and $\mathrm{nerf}(x)$ denotes the normalized error function $1/2 + 1/2\,\mathrm{errorf}(x)$. Figure 4(a) illustrates that this relation breaks down for deeper layers—mainly because of precession. Moreover, before precession sets in, a careful analysis reveals that the left-right symmetry of $\omega(r)$ is broken: the right (large r) tail of $\omega(r)$ is significantly steeper than its left (small r) tail for $H \gtrsim 0.45$.

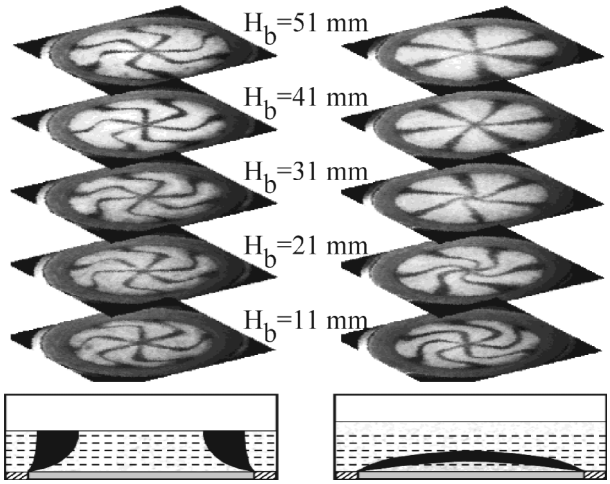

FIG. 3. 3D flow profiles around transition point. Left: Five slices for $H/R_s \simeq 0.6$ and heights H_b in the material as indicated—here $\omega_p \simeq 0$. The kink in the patterns corresponds the location of the shear zone. Right: Five slices at identical heights H_b for larger $H/R_s \simeq 0.75$, where $\omega_p \simeq 0.8$. The upper layers show no deformation of the pattern indicating the absence of shear. Below: Sketches of the shear zones within the bulk (black)—the dashed curves indicate the heights H_b where the patterns were created.

These changes in the *surface* profiles reflect the topological change in the 3D flow structure. For shallow layers, two flow profiles obtained for the same height H, but for two different slip radii (R_{s1} and R_{s2}), are simply related by a translation of the radial coordinate via $\omega(r - R_{s1})|_{R_{s1},H} = \omega(r - R_{s2})|_{R_{s2},H}$—the shear zone is a *local* phenomenon, insensitive to the location of the center of the shear cell [6]. For deep layers, when $\chi(r)$ becomes a nonlinear function, this symmetry is absent, since the flow is sensitive to where the center is—the shear mode is *global*. The precession and symmetry breaking of $\omega(r)$ both reflect the crossover from a local to a global shear mode—consistent with the change in the 3D structure of the shear zones.

To capture the symmetry breaking and precession, $\omega(r)$ could be fitted to a four parameter fit: $\omega(r) = p + (1 - p)\mathrm{nerf}[\lambda + s\lambda^2]$, where $\lambda = (r - R_c)/W$. Such fits confirm the independence of ω_p to details and the onset of symmetry breaking before precession. More insight can be gained when postulating that

$$\omega(r) = \mathrm{nerf}[\chi(r)], \tag{2}$$

and calculating $\chi(r) := \mathrm{nerf}^{-1}[\omega(r)]$ from our experimentally obtained velocity profiles. The resulting $\chi(r)$, shown in Fig. 4(b), clearly bring out the deviations from the simple form, Eq. (1). For shallow layers $\chi(r)$ is a linear function since $\omega(r)$ obeys Eq. (1): $\chi(r) = a_0 + a_1 r = (r - R_c)/W$. For deep layers, $\chi(r)$ becomes a nonlinear function that saturates at a precession-dependent value for $r \downarrow 0$. To fit $\chi(r)$ for deep layers, the most obvious choice is to add a symmetry breaking term $\sim r^2$—the resulting fit is rather poor. However, $\chi(r)$ can be fitted well by a cubic polynomial [see Fig. 4(b)]:

$$\chi(r) = a_0 + a_1 r + a_3 r^3. \tag{3}$$

We do not see strong *a priori* reasons why this fit would represent the true analytical form of the flow profiles. However, the surprise is that a_1 vanishes for large H (since the slope near the intercept becomes zero), while a_3 is zero for small H. Hence, by the addition of *one* fit parameter to the "pure" error-function form [Eq. (1)], $\omega(r)$ for both the shallow and deep regimes can be expressed in a simple form. Moreover, both precession and symmetry breaking are captured by this single extra parameter.

Location of the shear zone.—For shallow layers, where $\omega(r)$ is given by Eq. (1), the center location R_c is independent of the particle properties and was found to follow the simple scaling law [6]:

$$1 - R_c/R_s = (H/R_s)^{5/2}. \tag{4}$$

The recent theory of Unger *et al.* [7] predicts the location of the shear zones at the surface, R_{model}, for all layer depths and deviates from the scaling relation Eq. (4). In Fig. 5 our data for the center of the shear zones is compared to both the power law and Unger's numerical result. For general shear zones, there is no unique choice for the center and we have tested the following three definitions:

$$R_1 := \quad \text{where } \omega(r) = 0.5, \tag{5}$$

$$R_2 := \quad \text{where } \partial_r \omega(r) \text{ is maximal}, \tag{6}$$

$$R_3 := \quad \text{where } \partial_r[r\omega(r)] \text{ (strain rate) is maximal.} \tag{7}$$

For shallow layers, both R_1 and R_2 are better described by Eq. (4) than by R_{model}, while R_3 appears to be better described by R_{model}. For deep layers, the situation is more complicated, with neither model describing any of the three measured curves in detail.

Mesoscopic Scale.—While the onset of precession and location of the shear zones are set by the system scales H and R_s, the *width* of the shear zones are set by a mesoscopic

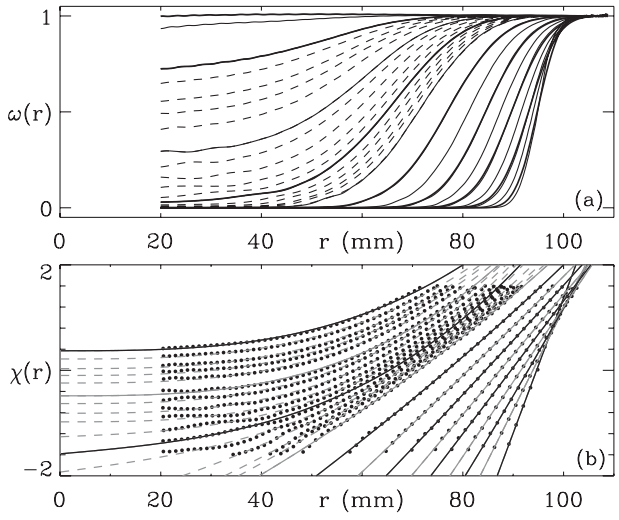

FIG. 4. Surface velocity profiles $\omega(r)$ for $R_s = 95$ mm and increasing layer depth H. Thick curves: $H = 10, 20, \ldots, 80$ mm; Thin curves $H = 15, 25, \ldots, 75$ mm; Dashed curves $H = 56, 57, \ldots, 69$ mm. (a) Precession gradually sets in for $H \gtrsim 60$ mm. (b) Corresponding profiles of $\chi(r)$ (dots), compared to cubic fits given by Eq. (3) (curves). Similar to panel (a), $H = 10, 15, 20, \ldots, 55, 56, \ldots, 70$ mm.

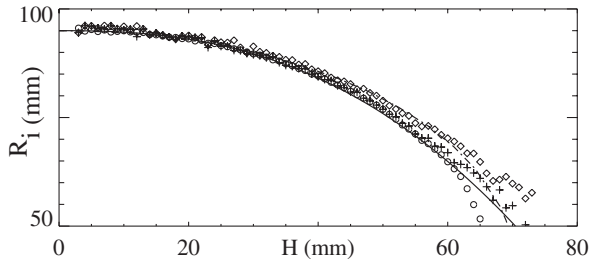

FIG. 5. Shear zone positions versus layer depth H for $R_s = 95$ mm, where circles, pluses, and diamonds correspond to R_1, R_2, and R_3 [Eqs. (5)–(7)]; the solid curve is the scaling form given by Eq. (4) and the dashed curve is the result by Unger *et al.* [7].

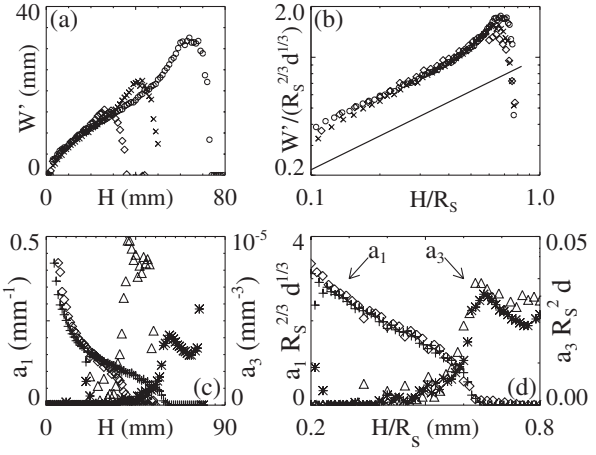

FIG. 6. (a) Width of shear zones W' as a function of H for $R_s = 45$, 65, and 95 mm. The saturation of W' for large H is related to the transition to precession—the eventual vanishing of W' is a fitting artefact caused by the flattening of the velocity profile. (b) The nondimensionalized width $W' R_s^{2/3} d^{1/3}$ follows a universal curve as a function of H/R_s, which for small heights is approximated well by a power law with exponent 2/3 (straight line). (c) Fit parameters a_1 for $R_s = 65$ mm (diamonds) and 95 mm (+) and a_3 for $R_s = 65$ mm (triangles) and 95 mm (stars) as a function of H. (d) Nondimensionalized fit parameters as a function of H/R_s (see text).

length scale governed by both H and grain size d. Earlier work for shallow layers was inconclusive about the *functional* dependence of the width on layer height [6]. To be able to discuss deep layers also, we define a width W' as the interval where ω grows from $\omega_p + 0.1 \times (1 - \omega_p)$ to $0.9 \times (1 - \omega_p)$—for shallow layers, $W' \approx 1.812W$ [see Eq. (1)]. We will now show strong evidence for a mesoscopic scale (Fig. 6), which grows as $H^{2/3}$ and which determines the width of the shear zones.

The first evidence comes directly from W'. For shallow layers, W' is independent of R_s, but for deep layers both the microscale (d) and macroscale (R_s) play a role [Fig. 6(a)]. When we postulate that the ratio of the relevant length scale to the grain size d (which we take as 0.7 mm) grows as $(H/d)^\alpha$, this suggests to plot the dimensionless width $W'/(R_s^\alpha d^{1-\alpha})$ as a function of the dimensionless height H/R_s and adjust α to get optimal collapse. As shown in Fig. 6(b), this leads to a good data collapse for $\alpha = 2/3$, and moreover, for shallow layers, the rescaled width itself grows as $(H/R_s)^{2/3}$. Secondly, the fit parameters a_1 and a_3, plotted in Fig. 6(c) for two values of R_s, have dimensions of inverse length and inverse length cubed. It follows that $a_1 R_s^{2/3} d^{1/3}$ and $a_3 R_s^2 d$ should collapse when plotted as a function of H/R_s, as is indeed the case [Fig. 6(d)].

Outlook and open questions.—Detailed studies of the granular flows in split bottom geometries [6–8] show a wide range of smooth and robust flows. Three regimes can be distinguished by fitting the surface flows to Eq. (1)–(3). *Shallow layers* occur for $H/R_s \lesssim 0.45$ where ω_p is zero, a_3 is zero and Eq. (1) fits the data well—here the shear zones completely reach the free surface [6]. For $0.45 \lesssim H/R_s \lesssim 0.65$, a crossover regime is reached where the left-right symmetry of $\omega(r)$ is broken, both a_1 and a_3 are nonzero but ω_p is essentially zero. *Deep layers* occur for $H/R_s \gtrsim 0.65$, where the reflection symmetry of the shear zones is strongly broken, precession sets in, a_1 tends to zero and where there is increasing shear in the vertical direction [8]. This robust behavior of grain flows in split bottom geometries will provide important testing ground for the development of (continuum) theories [7,9,10].

There are three questions that we think deserve particular attention. (i) What mechanism selects the functional form of $\omega(r)$? In particular, the tails of these profiles deserve special attention, since they can be exponential, Gaussian, or more complex as shown in Fig. 4 [3,6,11]. (ii) What sets the nontrivial exponent 2/3 for the scaling of the width of the shear zones? (iii) Should the transition to precession be conceived as a smooth crossover or as a sharply defined transition? The smooth growth of ω_p with H/R_s suggests a crossover (Fig. 2), while the (critical) vanishing of a_1 with (H/R_s) [Figs. 6(c) and 6(d)] suggests a sharp transition.

We gratefully acknowledge discussions with X. Cheng, H. Jaeger, S. Nagel, T. Unger, J. Kertesz, M. Depken, and W. van Saarloos, and financial support from "Nederlandse Organisatie voor Wetenschappelijk Onderzoek (NWO)" and "Stichting Fundamenteel Onderzoek der Materie (FOM)."

[1] GDR MiDi, Eur. Phys. J. E **14**, 341 (2004).
[2] R. Nedderman, *Statics and Kinematics of Granular Materials* (Cambridge University Press, Cambridge, England, 1992).
[3] D. M. Mueth *et al.*, Nature (London) **406**, 385 (2000); D. M. Mueth, Phys. Rev. E **67**, 011304 (2003).
[4] D. W. Howell, R. P. Behringer, and C. T. Veje, Phys. Rev. Lett. **82**, 5241 (1999).
[5] W. Losert, L. Bocquet, T. C. Lubensky, and J. P. Gollub, Phys. Rev. Lett. **85**, 1428 (2000); W. Losert and G. Kwon, Advances in Complex Systems **4**, 369 (2001); M. Toiya, J. Stambaugh, and W. Losert, Phys. Rev. Lett. **93**, 088001 (2004).
[6] D. Fenistein and M. van Hecke, Nature (London) **425**, 256 (2003); D. Fenistein, J.-W. van de Meent, and M. van Hecke, Phys. Rev. Lett. **92**, 094301 (2004).
[7] T. Unger, J. Török, J. Kertész, and D. E. Wolf, Phys. Rev. Lett. **92**, 214301 (2004).
[8] X. Cheng *et al.*, Phys. Rev. Lett. **96**, 038001 (2006).
[9] J. Kertész (private communications).
[10] M. Depken, W. van Saarloos, and M. van Hecke, Phys. Rev. E **73**, 031302 (2006).
[11] T. S. Komatsu, S. Inagaki, N. Nakagawa, and S. Nasuno, Phys. Rev. Lett. **86**, 1757 (2001).